Microwave Electromagnetic Field Sensor on Thin-Film Lithium Niobate Using Photonic Down-Conversion Detection

Gregory S. Kanter, *Member, IEEE*, Paul M. Moraw, K. F. Lee, Farzaneh Arab Juneghani, *Graduate Student Member, IEEE*, Milad Gholipour Vazimali, Kwangwoong Kim, Nicolas K. Fontaine, and Sasan Fathpour, *Senior Member, IEEE*

***Abstract*—We integrate a bow-tie antenna on a thin-film lithium niobate (TFLN) phase modulator to form an electromagnetic E-field sensor. The fiber-coupled TFLN chip is probed by a two-tone optical local oscillator generated using an external phase modulator, which after appropriate filtering allows the system to act as a photonic down-converter. The system is compatible with the use of balanced detection, enabling an improved signal-to-noise ratio. We demonstrate the down-conversion of a 28.3 GHz free-space microwave signal to 100 MHz with a sensitivity of 2 mV/m/$\sqrt{\text{Hz}}$. The current sensitivity limitation stems from the relatively high (25 dB) insertion loss of the packaged device, which is not inherent to the design. The technology can be directly scaled to much higher frequencies and is attractive for remote detection of microwave electromagnetic signals.**

***Index Terms*—Microwave photonics, E-field sensor, optical fiber communication, microwave measurement, microwave antennas.**

I. Introduction

ELECTRO-OPTICAL (EO) sensors have great potential for measuring electromagnetic signals. Such sensors can be fully passive and interfaced via low-weight, high-bandwidth, low-loss, and electromagnetic interference-free optical fiber. Moreover, the sensors themselves can be primarily dielectric, with only small levels [1] or even a complete absence [2] of metal content. These properties make them ideal for remotely monitoring electromagnetic signals, for instance in difficult-to-reach locations, in hostile environments, or for antenna characterization.

A common means of EO detection is via an intensity modulator, such as a Mach-Zehnder interferometer (MZI) modulator, defined on a material with high EO effect such as lithium niobate. In this case, an incoming electric field (E-field) causes an imbalanced phase change in the two arms of the interferometer, for instance, due to one arm being excited by an antenna [3] or the two arms having opposite poling [2]. The output optical intensity is then intensity modulated by the incoming electric field and can be photo-detected to create an electrical signal. The detected signal mirrors the incoming E-field so that the photodetector bandwidth should be as high as the desired E-field frequency to be measured.

General E-field measurements, such as often needed for applications in communications or radar, preserve both the amplitude and phase information of the incoming signal. Typically, such RF receivers convert the high frequency signal carrier (e.g., >10 GHz) into a lower intermediate frequency (IF; e.g., <1 GHz) in a process called down-conversion. Down-conversion makes the signal more manageable and compatible with low-cost, high-performance analog-to-digital converters (ADCs) enabling subsequent digital signal processing. Down-conversion in the RF domain typically requires an RF local oscillator (LO) near the signal frequency and has undesirable effects on the signal including LO leakage, loss, and distortion [4]. Moreover, for remote antennas the RF down-conversion system (including LO) should be co-located with the antenna so that the high carrier frequency does not need to be transmitted through significant lengths of electrical cable. An alternative implementation is a photonic down-conversion (PDC) [4], [5], [6] scheme which performs the frequency translation optically thereby eliminating the microwave mixer. Importantly, PDC gives much greater freedom in choosing the photodetectors since the central frequency of detection is now the lower IF.

While well-studied in RF-fiber links, E-field measurement systems have only rarely employed down-conversion and at comparatively low RF frequencies [7]. Instead, most sensors monitor the received signal directly by measuring the photo-detected signal on a high-frequency electrical spectrum analyzer (ESA) [8]. As the desired frequencies of detection increase and more advanced applications like radar or electromagnetic spectral monitoring become of interest, PDC should become an increasingly important tool.

An interesting RF-photonic PDC communication link that uses only phase modulation has previously been proposed and demonstrated [5]. In addition to the phase modulator that

Manuscript received 31 May 2023; revised 18 July 2023; accepted 31 July 2023. Date of publication 3 August 2023; date of current version 10 August 2023. This work was supported by the United States Air Force Research Lab under Contract FA864921P1501. *(Corresponding author: Gregory S. Kanter.)*

Gregory S. Kanter, Paul M. Moraw, and K. F. Lee are with the NuCrypt, LLC, Park Ridge, IL 60068 USA (e-mail: kanterg@nucrypt.net).

Farzaneh Arab Juneghani, Milad Gholipour Vazimali, and Sasan Fathpour are with the CREOL, The College of Optics and Photonics, University of Central Florida, Orlando, FL 32816 USA.

Kwangwoong Kim and Nicolas K. Fontaine are with the Nokia Bell Labs, Murray Hill, NJ 07974 USA.

Digital Object Identifier 10.1109/JPHOT.2023.3301446

modulates the incoming signal to be measured, this system also uses a second phase modulator to apply an RF LO, followed by a notch filter to remove the original optical carrier. The detected IF is then at the absolute frequency difference between the LO and the incoming signal. A single photodetector can then measure the down-converted signal. Unlike MZI's, phase modulators do not require a DC bias and in principle preserve the full optical power of the input (MZI's can preserve the full optical power if they have dual outputs, but this requires more complex fiber coupling and management). These properties make phase modulators good candidates for remote signal monitoring. Additionally, cascading phase modulators into an array can lead to a higher modulation index and thus more sensitive detection [1].

Another PDC method generated a two-tone optical LO using an MZI biased for carrier suppression [9]. This creates two optical tones separated by twice the frequency driving the MZI. A benefit of this method is that the required RF frequency used to generate the optical LO is reduced by a factor of two, thus easing the burden of detecting high microwave frequencies. The optical two-tone LO feeds a phase modulator that is modulated by a microwave signal, then the optical bands surrounding the two LO tones are separated in a programmable optical filter and detected in a balanced photo-detector (BPD). The BPD subtracts out common mode noise and increases the net optical power that can be received before nonlinear distortions occur. A related two-tone PDC experiment has demonstrated PDC to be useful for free space links [10]. Free-space RF reception is possible by connecting an external antenna, such as a horn antenna, to a typical receive-side optical modulator that uses traveling wave co-planer RF electrodes [11].

The high EO modulation index and mature technology base of lithium niobate make it a well-used platform for E-field sensing without the use of an external antenna. Such sensors commonly either have micro-antennas integrated into the same chip as the optics [3], or they imprint the incoming E-field onto the optical field directly by appropriate design, such as controlled poling [2]. The last decade has seen a surge in the development of thin-film lithium niobate (TFLN), in particular for communications applications, as it promises smaller and more integratable devices as well as high-bandwidth and high-efficiency (low V_π) modulation [11], [12]. TFLN has been adapted for use in E-field sensing as well [13], [14], [15], which is sensible as this application should benefit from the same properties that make it so appealing for use in optical communications. However, other than preliminary work by the authors [16], to our knowledge all TFLN E-field sensors demonstrated thus far are intensity modulators, and no TFLN E-field sensors have been used with PDC.

In this work, we demonstrate a TFLN-based E-field sensor based on an integrated bow-tie antenna coupled to a phase modulator. The largest dimension of the antenna is 1.85 mm and it is designed for use between 20-36 GHz. The sensor is probed by a two-tone optical signal generated by passing laser light through an external phase modulator driven at 14.1 GHz. The optical output from the sensor is optically amplified and separated into two ports using a commercial 2.5 GHz asymmetric MZI (AMZI) demodulator (commonly used for the detection of differential phase-shift-keyed communications), and each output is detected in a BPD. This scheme is used to photonically down-convert a 28.3 GHz incoming microwave signal to a 100 MHz IF signal. We show the benefit of balanced detection by comparing the performance using just one of the asymmetric demodulator ports to that of using both ports. The increase in gain from using both ports is larger than the increase in the noise floor, leading to an improvement in signal-to-noise ratio (SNR). Sensitivity to an incoming electric field in the far-field of a horn antenna is about 2 mV/m/$\sqrt{\text{Hz}}$. The sensitivity is encumbered by the 25 dB insertion loss of the packaged antenna, which limits the optical power that can be sent to an erbium-doped fiber amplifier (EDFA) used to boost the optical power before the detection apparatus. The associated relative intensity noise (RIN) from this EDFA is the dominant source of noise. However, the waveguide propagation loss of 2.6 dB/cm and simulated loss through the antenna structure of $<$0.1 dB suggests the losses are dominated by technical loss such as mode matching at the fiber/facet interface. TFLN facet coupling losses are more commonly $<$5 dB/facet [17], with recent work demonstrating sub-dB/facet [18]. Thus, substantial improvements in sensitivity are to be expected with greater attention to coupling loss.

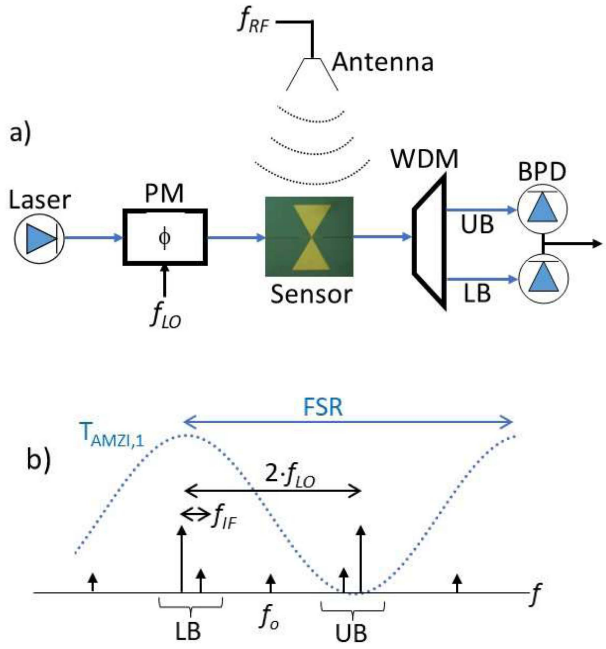

Fig. 1. (a) Simplified diagram of TTDC probing of an E-field sensor. (b) Conceptual diagram of the optical spectrum into the AMZI (*x*-axis is optical frequency) acting as a WDM. One of the two AMZI output transmissivity functions is overlayed as a dotted line ($T_{AMZI,1}$). This output is set to pass the LB and block the UB. The other AMZI output has an inverted transmissivity function (pass the UB, block the LB). We set $N = 0$ in the figure for clarity.

II. Operating Principle

A simplified conceptual diagram of a two-tone down-conversion (TTDC) system is depicted in Fig. 1. A two-toned optical LO signal used for probing the sensor is generated by modulating a laser via an external phase modulator (PM) with a sinusoid at frequency $f_{LO} = (f_{RF} \pm f_{IF})/2$, where f_{RF} is

the central RF frequency to be detected and f_{IF} is the desired IF frequency. The phase modulation creates symmetric optical tones about the carrier, separated by integer multiples f_{LO}.The tone power can be calculated for a given modulation index using the Bessel function. For instance, a modulation index of $m_0 = 1.84$ would generate two first-order spectral tones of intensity $I_0 \cdot (J_1(1.84))^2 = 0.339 \cdot I_0$, where I_0 is the output intensity of an unmodulated laser through the LO-PM and J_x is the Bessel function of order x. This LO generation configuration generates maximum power in the two 1st-order tones ($f_0 \pm f_{\mathrm{LO}}$), but also keeps $(J_0(1.84))^2 = 10\%$ of the power in the carrier and $(J_2(1.84))^2 = 10\%$ of the power in each of the 2nd-order tones. We note that if the 2nd order tones are filtered out with a band-pass filter, the main implication of undesired tones is the optical loss that they represent. If they are not filtered out, then their implication is more complicated, but it is a secondary effect that is neglected in this analysis.

The RF signal to be measured centered at frequency f_{RF} is sent to a transmit antenna, which generates a propagating E-field that is directed to the sensor. The sensor contains a bow-tie antenna that is designed to induce an electric field across a short gap containing an optical waveguide. The electro-optic effect causes the induced electric field to phase-modulate the two-toned optical LO. A conceptual graphical depiction of the resulting optical spectrum is shown in Fig. 1(b), where only the carrier and first-order tones are considered, and we arbitrarily set $f_{\mathrm{RF}} < 2 \cdot f_{\mathrm{LO}}$. The optical spectrum consists of an upper band (UB) around $(f_0 + f_{\mathrm{LO}})$ and a lower band (LB) around $(f_0 - f_{\mathrm{LO}})$. Each band generates a beat frequency of f_{IF}, but they are 180° out-of-phase thus canceling out and leaving no intensity modulation (as expected for a phase modulator). However, if the two bands are separated, such as by using a wavelength division multiplexer (WDM), then either band can be detected by a photodetector and will lead to a detected signal at the IF. Additionally, the IF signals from each band will be out-of-phase with the other, so subtracting them in a balanced detector will ideally double the detected current leading to a 6 dB increase in signal power. Assuming the noise is uncorrelated in the two bands, the subtracted noise power level is only increased by 3 dB leading to a 3 dB nominal improved signal-to-noise ratio (SNR). Some types of noise, such as relative intensity noise (RIN) from the laser, can be correlated in both bands. This common-mode noise can subtract out and therefore even further improve SNR [19].

The two bands can be separated using technologies such as add-drop multiplexing (ADM) filters. Typical low-loss filtering technologies have bandwidths >0.1 nm (12.5 GHz for a 1550 nm wavelength), making them well-suited for separating bands that are spaced by many 10's of GHz. The tones can also be separated using an asymmetric Mach-Zehnder interferometer (AMZI). Here, the internal phase of the AMZI periodic filter is set to pass the UB to one output port and the LB to another. We note the AMZI is simply a waveband-splitting tool and is not particularly sensitive to laser line-width. To effectively separate the bands of interest, the free spectral range (FSR) of the AMZI should be such that $(N + 0.5) \cdot \mathrm{FSR} \approx 2 \cdot f_{\mathrm{LO}}$, where N is a non-negative integer representing the number of excess FSR intervals between

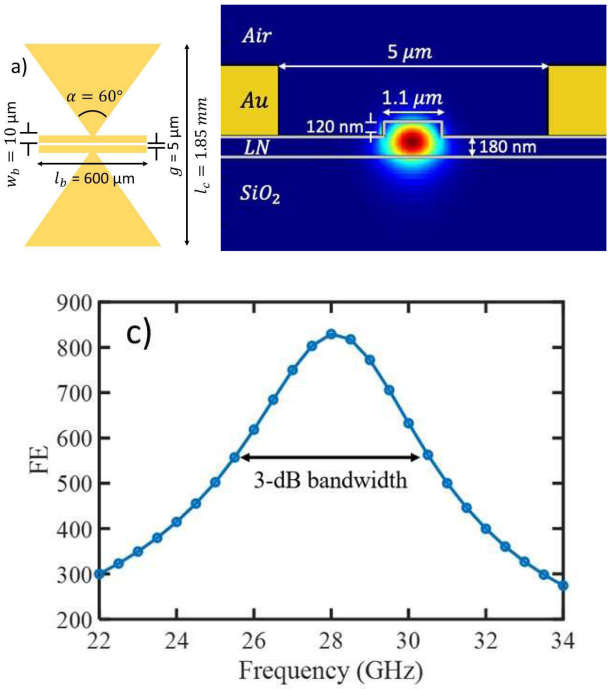

Fig. 2. (a) Geometry of the bow-tie antenna. The optical waveguide is located in the central gap. (b) Cross-sectional view of the chip (c) Simulated FE of the antenna as a function of RF frequency. The 3-dB bandwidth is shown for the square of the FE, which is the power bandwidth.

the UB and LB. Each band is then detected using a different port of the BPD, which generates an output at the IF.

Fig. 2(a) shows the basic geometry of the bow-tie antenna on a TFLN platform on silicon substrates and Fig. 2(b) shows the waveguide cross-section of a rib-loaded TFLN waveguide with single-mode operation. The antenna receives an RF signal and induces a strong electric field between two electrodes separated by 5 μm. The antenna has been designed for maximum field enhancement (FE) at 28 GHz. The FE factor is defined as the ratio of the induced electric field inside the gap between the electrodes to the incident electric field [1]. A simulated curve showing the expected FE as a function of frequency is shown in Fig. 2(c). Ansys Lumerical is primarily used for optical simulations, while COMSOL Multiphysics is used for microwave/RF simulations.

The bandwidth of the proposed antenna is defined as the square of the FE to represent performance in terms of RF power. The simulated 3-dB bandwidth is 5 GHz with a FE factor equal to 830 at the center frequency of 28 GHz. An optical waveguide is defined between the electrode gap region and the electric field is imprinted onto the phase of the optical carrier confined in the waveguide via the exploited r_{33} electro-optic coefficient.

The wafer's silicon substrate possesses a high resistivity (>10000 $\Omega \cdot$cm) that makes it a semi-conductive material which is essential for high-frequency and high-speed applications. Fig. 3(a) shows a 3D representation of the antenna's far-field pattern, obtained using the CST Studio suite. Fig. 3(b) shows a corresponding polar representation in the E-plane. While the radiation pattern is asymmetric in the vertical direction, the antenna gain is 0.4 dBi in the forward direction, resulting in

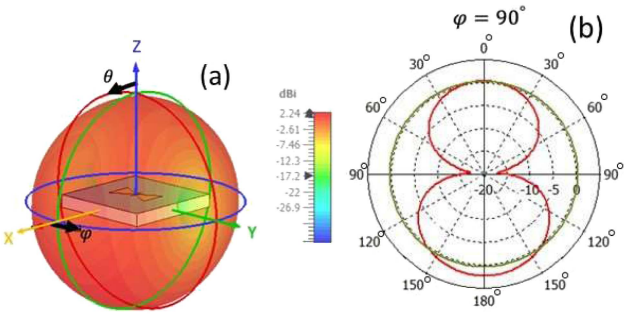

Fig. 3. Simulation of antenna far field. (a) 3D rendering. (b) E-plane polar plot. The radial axes are in dBi units.

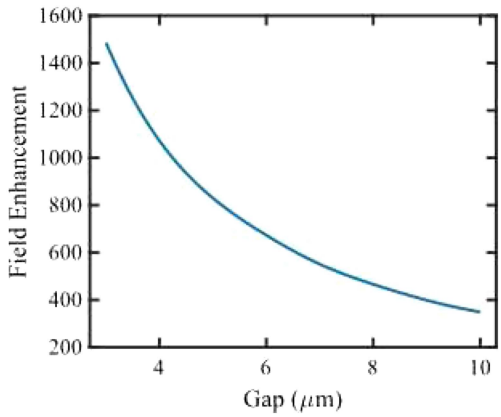

Fig. 4. Simulation of FE vs. electrode gap.

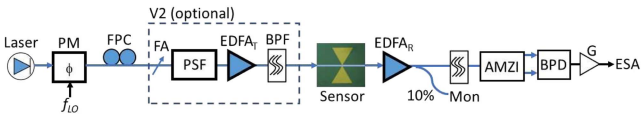

Fig. 5. Experimental configuration also shows the optional insert used for experimental version 2 (V2). G is an electrical amplifier, Mon is a monitor port, FA is a fixed attenuator (used to protect the PSF from high power levels).

a pattern that for the purposes of our experiment is close to an omnidirectional pattern.

Fig. 4 shows a simulation of the FE factor as a function of the gap between the electrodes. A gap of 5 μm was chosen as a conservative value to keep optical loss due to the near-by metal negligible. It is an open design issue to choose the gap so as to find a desirable trade-off between FE and optical loss.

III. Experiment

An experimental diagram of the PDC E-field sensor experiment is shown in Fig. 5. An optional subsystem is highlighted, which consists of a fixed attenuator (FA), programmable spectral filter (PSF realized by a Finisar Waveshaper filter), a transmit-side EDFA, and a band pass filter (BPF) to remove excess amplified spontaneous emission noise (ASE). This optional subsystem is removed in version 1 (V1) of the experiment and inserted in version 2 (V2), as described further below.

Fig. 6. Photograph of the packaged chip, shown without a removable plastic cover. Note the plastic cover is attached during the measurement while the metal screws securing the white plastic mount in the photo are not present.

A horn antenna with a gain estimated from the datasheet as $G = 21.4$ dB (at 28 GHz) is excited by an RF signal. The magnitude of the RF signal fed to the horn is controlled by changing the output power of a programmable signal generator that feeds a chain of components, consisting of a frequency doubler, a high-pass filter, an electrical amplifier, and a 10-dB attenuator. The power delivered to the horn antenna P_T at a given signal generator power setting is estimated using a power detector (Mini-Circuits ZV47-KR44). The 5.4×4.2 cm^2 aperture of the horn is mounted at $R = 99$ cm above the sensor. Specifying the far field condition as $2 \cdot {D_{min}}^2/\lambda$, where D_{min} is the minimum aperture dimension and λ is the RF wavelength, we find the sensor is well outside the 33 cm far field range and thus calculate the power density at the sensor as $P_d = G \cdot P_T/(4\pi \cdot R^2)$ [8].

A laser with 19 dBm output power near 1552 nm (APIC LN-1550-168-80) is phase modulated at $f_{LO} = 14.1$ GHz. The relative size of the resulting spectral tones observed on an optical spectrum analyzer (OSA; HP 86140A) with 0.06 nm resolution bandwidth is consistent with a modulation index of $m = 1.85$, with the desired 1st order tones at $(f_o \pm f_{LO})$ about $3\times$ larger than the output laser tone or the 2nd order tones. A fiber polarization controller (FPC) is adjusted so that the transverse-electric (TE) mode of the waveguide is excited. The fiber-coupled packaged sensor chip shown in Fig. 6 has 25 dB fiber-to-fiber insertion loss. Measurements of a ring resonator on the same chip suggest the propagation loss of the waveguide is 2.6 dB/cm. The net waveguide length of 0.9 cm and the anticipated 0.7 dB reflection loss per facet suggests the average coupling loss per facet is 10.6 dB. End-to-end losses of about 14 dB have been obtained pre-packaging using high-precision stages to couple light from lensed fibers through the chip soon after fabrication. Thus, we believe the high insertion loss is largely due to technical issues such as poor mode-matching or some kind of contamination.

The optical output from the sensor is amplified in a receive-side EDFA (EDFA$_{\mathrm{R}}$, Lightwaves2020 NOAPF252R), band-pass filtered to limit out-of-band ASE noise, then sent to an AMZI for separating the upper and lower bands. The AMZI is a commercially available device (Optoplex DPSK demodulator) with a nominal 2.5 GHz FSR. This allows for operation at a variety of RF signal frequencies spaced by about 1.25 GHz. The internal phase of the AMZI is adjustable via a bias voltage that controls the temperature of the device. For $N = 11$, we expect the optimal $f_{LO} = 14.375$ GHz, though we found experimentally

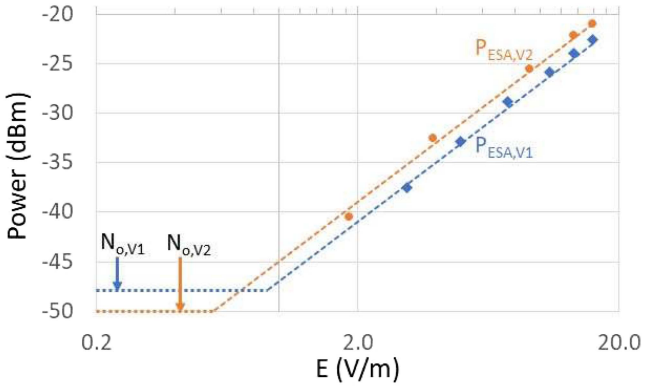

Fig. 7. Linearity plot of the peak IF signal power measured near 100 MHz on the ESA for both the V1 and V2 configurations (see labels) as a function of the incident electric field. The noise levels in a resolution bandwidth of 100 kHz are depicted with a dotted line and dashed lines fit the data with a fixed slope of 2 on a log scale.

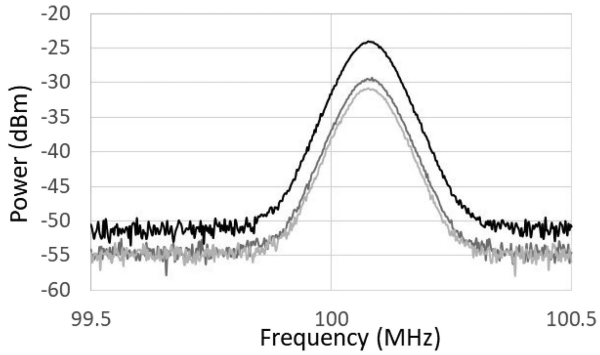

Fig. 8. ESA trace of a balanced detection measurement (black), and with both outputs measured single-ended (grey and light grey).

that $f_{LO} = 14.1$ GHz allowed the two 1st-order tones to be more cleanly separated.

The outputs of the AMZI were fed into the BPD (Thorlabs BDX1) and amplified by a chain of amplifiers with a net gain at 100 MHz of 46.4 dB. The power measured by an ESA (Agilent N9320A) in a 100 kHz resolution bandwidth is measured while varying P_T. Fig. 7 plots the noise-floor corrected IF power as a function of the inferred E-field at the sensor. The relationship follows the expected linearity trend, where every dB change in E-field changes the received power by 2 dB. The intersection of the linear fit of the signal power with the noise floor gives a sensitivity of 0.89 mV/m/$\sqrt{}$100 kHz or equivalently 2.8 mV/m/$\sqrt{}$Hz.

We can define a captured power level relative to an isotropic antenna as $P_c = P_d \cdot \lambda^2/(4\cdot\pi)$ [1], which allows us to convert the -48 dBm noise floor and the net system gain of 2.7 dB (which includes the gain of the electrical amplifiers) into a relative noise figure, NF $= 10\cdot\log_{10}\{N_{out,1Hz}/(G\cdot kT)\} = -73.2$ dB, where $N_{out,1Hz}$ is the output noise floor in a 1 Hz bandwidth, k is Boltzman's constant and $T = 293$ K is room temperature [20]. It is expected that the noise floor is primarily due to the low power entering EDFA$_{\rm R}$ of $P_{o,in} = -17.7$ dBm/tone, as this is considerably smaller than the power hitting either detector which is approximately -1 dBm. This can be further justified by calculating the expected noise floor assuming RIN from the signal-spontaneous beat noise from EDFA$_{\rm R}$ is the only noise source, which can be estimated [20] using $\text{RIN}_{\text{sig-sp}} = \frac{4n_{sp}hf}{P_{o,in}}$, where n_{sp} is the amplifier spontaneous noise emission factor which we set to the ideal value of $n_{sp} = 1$ (signifying a 3 dB amplifier noise figure), and hf is the energy of a photon. This leads to a minimum estimated $\text{RIN}_{\text{sig-sp}} = -135.2$ dBc, which can be translated into a noise floor $N_{out,1Hz} = \text{RIN}\cdot \text{I}_{\text{DC}}{}^2 \cdot R_{\text{out}}$, where I_{DC} is the net current of the detector and R_{out} is the load resistance [20]. Using the 1 A/W nominal conversion efficiency of the detectors, a 2 dBm net power level (including both detectors), and $R_{\text{out}} = 50$ ohm leads to an estimated noise floor, after accounting for eletrical gain, of $N_{\text{out,100kHz}} = -47.8$ dBm, which is consistent with the experiment and supports the claim that $\text{RIN}_{\text{sig-sp}}$ is the dominant noise source.

The optional optical sub-system depicted in Fig. 5 was added to realize the V2 experiment with the goal being to improve SNR by increasing the optical power of the 1st-order tones entering EDFA$_{\rm R}$. This is accomplished by using the PSF as a dual-band filter to pass the $\pm$1st order tones and attenuate the other tones. This filtering better isolates the optical power in the spectral region of interest maximizing the power available from a saturated EDFA. We amplify these tones in a pre-sensor EDFA. The power-per-tone into EDFA$_{\rm T}$ and EDFA$_{\rm R}$ is -1 dBm and -12.2 dBm, respectively. The net noise level is thus still expected to be dominated by EDFA$_{\rm R}$, but the optical power level pre-EDFA$_{\rm R}$ has been increased by 5.5 dB in changing to the V2 configuration. Given that nearly half of the optical power is now in each of the first order tones, the net power sent to the waveguide is about 16 dBm. Fig. 7 also shows linearity data from V2. We note that in V2 the photo-detected powers are about 2 dB higher leading to higher gain but the noise floor has actually fallen to -50 dBm/100 kHz. The combined 1.7 dB higher gain and 2 dB lower noise floor leads to an SNR and NF improvement of 3.7 dB, or a sensitivity of 1.8 mV/m/$\sqrt{}$Hz.

Fig. 8 shows a set of spectral measurements from the ESA recorded with the BPD receiving both AMZI output ports (balanced configuration) or just one or the other port (single-ended configuration). Comparing the SNR of the balanced detection data to the average single-ended data shows an improvement of 2.5 dB demonstrating the value of balanced detection. The 2.5 dB improvement is reasonably close to the anticipated 3 dB improvement, and the somewhat reduced value could be attributable to various experimental factors including imperfect balancing of the currents from the detectors.

The impact of received optical power is assessed by measuring the SNR at a fixed E-field of 13.5 V/m, while the power to the detectors is varied using a variable optical attenuator (VOA) inserted before the AMZI. The loss of the uncalibrated VOA is assessed by taking the data in a single-ended configuration (only one AMZI output was connected to the BPD) and monitoring the power of the other AMZI output channel on an OSA. Measurements are taken over a 5 dB range of VOA insertion losses. As expected, the measured ESA RF power level changes by 2 dB per dB of received optical power (since optical power is linearly related to current and RF power is proportional to the current squared), but the noise level also changes by the same amount.

That is, in this power range the SNR is not sensitive to the power received by the photodetector. This characteristic is consistent with RIN-limited noise levels verifying that we are still limited by the power levels entering $EDFA_R$. It also demonstrates that the SNR benefit of balanced detection seen in Fig. 8 is not simply attributable to the increased current from the photodetector.

IV. Conclusion

We demonstrated a TFLN E-field sensor based on a bow-tie antenna acting as an optical phase modulator. Such a sensor requires no biasing and is fully electrically passive with only optical fiber interconnects. The simple antenna structure and small size (1.85 mm maximum dimension) make it well-suited for remote detection, as well as for future applications where multiple antennas are integrated on a single chip. A two-tone optical LO probes the sensor, down-converting the 28.3 GHz incoming E-field into a 100 MHz IF signal. The two-toned LO is created using an external optical phase modulator driven at 14.1 GHz. The two tones are separated off-chip using an AMZI optical filter allowing for the incoming signal to be recovered at the 100 MHz IF. Improved performance via the use of balanced detection of both tones is observed. The relatively low LO driving frequency is an advantage for scaling the technique to yet higher microwave detection frequencies such as the W-band (75–110 GHz). The technical difficulties in detecting, processing, and measuring microwave signals at such high carrier frequencies make the photonic down-conversion technique particularly appealing, with the only substantial changes from the current experiment being scaling down the antenna dimensions (which in any case are far larger than the optical dimensions and are thus trivial to fabricate) and using an LO modulator (in our case a phase modulator) with a bandwidth of $\sim$50 GHz. Such modulators are commercially available. Seeing that modulators operating at $>$100 GHz have been reported [12], [21], even further scaling the measurement frequency to 100's of GHz is within reach.

E-field detection sensitivities down to 2 mV/m/$\sqrt{\text{Hz}}$ is observed, with the limitation coming from RIN noise from an optical pre-amplifier. This noise is exacerbated by the 25 dB insertion loss of the packaged sensor that causes the optical power into the EDFA to dip into low levels. The high insertion loss is not inherent to the design, and it is expected that $\sim$20 dB improvement is possible which would lead directly to a similar level of noise reduction. Further improvements in sensitivity are expected by optimizing the sensor design, including the use of quartz as a substrate [22], and by the use of cascaded antenna arrays [1].

Acknowledgment

Any opinions, findings and conclusions or recommendations expressed in this material are those of the author (s) and do not necessarily reflect the views of the United States Air Force.

References

[1] D. H. Park, V. R. Pagán, T. E. Murphy, J. Luo, A. K.-Y. Jen, and W. N. Herman, "Free space millimeter wave-coupled electro-optic high speed nonlinear polymer phase modulator with in-plane slotted patch antennas," *Opt. Exp.*, vol. 23, no. 7, pp. 9464–9476, Apr. 2015.

[2] D. H. Naghski, J. T. Boyd, H. E. Jackson, S. Sriram, S. A. Kingsley, and J. Latess, "An integrated photonic Mach-Zehnder interferometer with no electrodes for sensing electric fields," *J. Lightw. Technol.*, vol. 12, no. 6, pp. 1092–1098, Jun. 1994.

[3] J. Zhang, Z. Zhao, C. Li, and Y. Li, "Broad-band integrated optical electric field sensor using reflection Mach-Zehnder waveguide modulator," *Fiber Integr. Opt.*, vol. 36, no. 4/5, pp. 157–164, Sep. 2017.

[4] Z. Tang, Y. Li, J. Yao, and S. Pan., "Photonics-based microwave frequency mixing: Methodology and applications," *Laser Photon. Rev.*, vol. 14, no. 1, Jan. 2020, Art. no. 1800350.

[5] V. R. Pagán, B. M. Haas, and T. E. Murphy, "Linearized electrooptic microwave downconversion using phase modulation and optical filtering," *Opt. Exp.*, vol. 19, no. 2, pp. 883–895, Jan. 2011.

[6] E. H. W. Chan and R. A. Minasian, "Microwave photonic downconverter with high conversion efficiency," *J. Lightw. Technol.*, vol. 30, no. 23, pp. 3580–3585, Dec. 2012.

[7] W. C. Wang, H. Lotem, R. Forber, and K. Bui, "Optical electric-field sensors," *Opt. Eng.*, vol. 45, no. 12, pp. 124402–124402, Dec. 2006.

[8] H. Lu, Y. Li, and J. Zhang, "Design and analysis of broadband $LiNbO_3$ optical waveguide electric field sensor with tapered antenna," *Sensors*, vol. 21, no. 11, May 2021, Art. no. 3672.

[9] P. Li, R. Shi, M. Chen, H. Chen, S. Yang, and S. Xie, "Linearized photonic IF downconversion of analog microwave signals based on balanced detection and digital signal post-processing," in *Proc. IEEE Int. Topical Meeting Microw. Photon.*, 2012, pp. 68–71.

[10] P. T. Dat et al., "Transparent fiber–millimeter-wave–fiber system in 100-GHz band using optical modulator and photonic down-conversion," *J. Lightw. Technol.*, vol. 40, no. 5, pp. 1483–1493, Mar. 2022.

[11] A. Rao et al., "High-performance and linear thin-film lithium niobate Mach–Zehnder modulators on silicon up to 50 GHz," *Opt. Lett.*, vol. 41, no. 24, pp. 5700–5703, Dec. 2016.

[12] P. O. Weigel et al., "Bonded thin film lithium niobate modulator on a silicon photonics platform exceeding 100 GHz 3-dB electrical modulation bandwidth," *Opt. Exp.*, vol. 26, no. 18, pp. 23728–23739, Sep. 2018.

[13] Y. Xue, Z. Ruan, and L. Liu, "Electrode-free photonic electric field sensor on thin film lithium niobate with high sensitivity," *Opt. Lett.*, vol. 47, no. 8, pp. 2097–2100, Apr. 2022.

[14] S. Toroghi and P. Rabiei, "Thin film lithium niobate electric field sensors," *Rev. Sci. Instrum.*, vol. 93, no. 3, Mar. 2022, Art. no. 034702.

[15] J. E. Toney, V. E. Stenger, S. A. Kingsley, A. Pollick, S. Sriram, and E. Taylor, "Advanced materials and device technology for photonic electric field sensors," *Proc. SPIE*, vol. 8519, pp. 11–22, Oct. 2012.

[16] F. A. Juneghani, M. G. Vazimali, K. F. Lee, G. S. Kanter, and S. Fathpour, "Integrated microwave-to-optical converter using patch antennas on thin-film lithium niobate," in *Proc. IEEE Int. Topical Meeting Microw. Photon.*, 2022, pp. 1–4.

[17] Y. Liu, H. Li, J. Liu, S. Tan, Q. Lu, and W. Guo, "Low V π thin-film lithium niobate modulator fabricated with photolithography," *Opt. Exp.*, vol. 29, no. 5, pp. 6320–6329, Mar. 2021.

[18] P. Ying et al., "Low-loss edge-coupling thin-film lithium niobate modulator with an efficient phase shifter," *Opt. Lett.*, vol. 46, no. 6, pp. 1478–1481, Mar. 2021.

[19] M. Schwerdt, J. Berger, B. Schuppert, and K. Petermann, "Integrated optical E-field sensors with a balanced detection scheme," *IEEE Trans. Electromagn. Compat.*, vol. 39, no. 4, pp. 386–390, Nov. 1997.

[20] V. J. Urick et al., "Long-haul analog photonics," *J. Lightw. Technol.*, vol. 29, no. 8, pp. 1182–1205, Apr. 2011.

[21] F. A. Juneghani et al., "Thin-film lithium niobate optical modulators with an extrapolated bandwidth of 170 GHz," *Adv. Photon. Res.*, vol. 4, no. 1, 2022, Art. no. 2200216.

[22] F. A. Juneghani, M. G. Vazimali, G. S. Kanter, and S. Fathpour, "Integrated electro-optical sensors for microwave photonic applications on thin-film lithium niobate," in *Proc. Int. Topical Meeting Microw. Photon.*, 2021, pp. 1–4.